Final Draft
of the original manuscript:

Laipple, D.; Wang, L.; Rackel, M.; Stark, A.; Schwebke, B.; Schreyer, A.; Pyczak, F.:

Microstructure of gas atomised Gamma-TiAl based alloy powders

In: MRS Advances (2017) Cambridge University Press

DOI: 10.1557/adv.2017.88

Microstructure of gas atomised γ-TiAl based alloy powders

Daniel Laipple[1], Li Wang[1], Marcus Rackel[1], Andreas Stark[1], Bernd Schwebke[1,2], Andreas Schreyer[1,3] and Florian Pyczak[1]
[1] Institute of Materials Research, Helmholtz-Zentrum Geesthacht, 21502 Geesthacht, Germany
[2] Institut für Werkstoffkunde und Werkstofftechnik, TU Clausthal, 38678 Clausthal-Zellerfeld
[3] European Spallation Source ERIC, P.O. Box 176, SE-221 00 Lund, Sweden

ABSTRACT

Due to the rapid development of advanced additive manufacturing production routes in recent years, the demand of high-quality alloy powders is significantly increased. We studied gas-atomised spherical powders of several Nb-bearing γ-TiAl based alloys, Ti-45Al-10Nb and Ti-45Al-5Nb-xC in at.% (x = 0, 0.5, 0.75, and 1), which were produced using the plasma melting induction guided gas atomization (PIGA) technique. The phase constitution of different powder fractions was determined by synchrotron high-energy X-ray diffraction at the HEMS beamline DESY (Germany), as well as by SEM, EDX and EBSD measurements. Due to the high cooling rates in the range of 10^5 K/s, the powder particles mainly consist of hexagonal close packed α-Ti(Al) and body centred cubic β-Ti(Al)-phase. As the cooling rate depends on the particle size, considerable amounts of the β-phase were only found in the small powder fractions (< 45 µm). The total β-phase amount was generally higher in the alloy with a higher Nb content, and also the effect of carbon as a α_2-stabilizer was observed. Dendritic cauliflower-like structures are more pronounced in bigger powder particles due to the slower solidification and thus a higher Nb depletion in the remaining melt.

INTRODUCTION

Currently, the interest in powder metallurgical (PM) processing routes, like additive manufacturing or metal injection molding is rapidly increasing. These techniques offer several advantages compared to conventional production techniques, such as near-net-shape production, possibility to generate complex geometries, high efficiency in material use, or high chemical homogeneity. The quality of the used powder, e.g. the purity, the size distribution, the particle shape or the phase composition, plays a decisive role for PM processing and for the properties of the final product.

Gas atomization is a process which produces metallic powder particles far from thermodynamic equilibrium due to the inherent high cooling rates in the range of 10^5 K/s to 10^6 K/s [1]. Usually a more or less broad distribution of powder particle sizes results and the actual cooling rate varies with powder particle size. Thus, different powder particle sizes may provide snapshots of rapidly quenched non-equilibrium microstructures for different cooling rates. Such differences in the microstructure of different powder particle size fractions may influence later processing steps by altering diffusion rates or mechanical properties.

We studied powders of Nb-rich γ-TiAl alloys, an upcoming material for aviation and automotive applications at elevated temperatures. Recently, γ-TiAl alloys are introduced as low pressure turbine blade material in civil aircraft engines [2] and first research activities were already started to introduce γ-TiAl powders in PM productions techniques [3,4,5]. We characterised the microstructure of different powder particle size fractions of several alloy

compositions by advanced microscopy and diffraction methods. This study is a detailed investigation of powder particles of Nb-rich γ-TiAl alloys directly after gas atomisation using Ar and is focused on the influence of the high cooling rate on phase composition and microstructure formed after quenching.

EXPERIMENTAL

Gas-atomised spherical powders of Ti-45Al-5Nb-xC (x = 0, 0.5, 0.75 and 1) and Ti-45Al-10Nb (all compositions in at.%) were produced in-house using the plasma melting induction guided gas atomisation (PIGA) technique [1]. The impurity levels in nitrogen and oxygen ranged around 100 mg/g and 400 mg/g, respectively and were analyzed using a conventional LECO melt extraction system. A typical particle size distribution generated by this technique is d_{50}~90 µm, 85 wt% < 180 µm and 19 wt% < 45 µm as shown in figure 1.

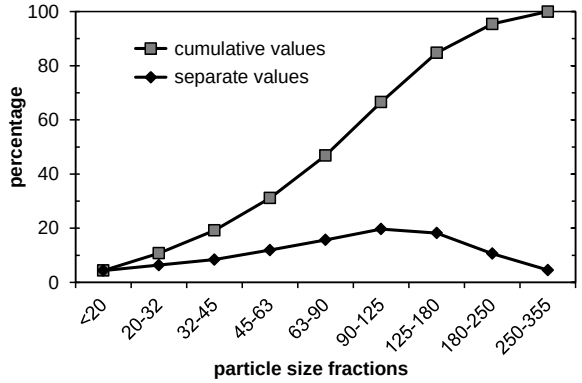

Figure 1: Mesh analysis in mass percent of Ti-45Al-5Nb powder fractions in µm, produced by PIGA.

The phase composition was determined by high-energy X-ray diffraction (HEXRD) performed at the high-energy synchrotron beamline HEMS of the Helmholtz-Zentrum Geesthacht at Petra III, DESY (Hamburg, Germany). Powder particles of different size fractions were filled in glass tubes with an inner diameter of 4 mm. The HEXRD measurements were performed in transmission mode with a photon energy of 87.3 keV (λ=0.142 Å) and a beam size of 0.5 × 0.5 mm. The resulting Debye-Scherrer-rings were recorded with a 2-dimensional mar345 image plate detector. The diffraction data were processed using the software fit2D [6] while the subsequent data evaluation by Rietveld analysis was done with powdercell 2.4 [7].

A crossbeam workstation AURIGA 40 from Zeiss (Oberkochen, Germany) was used for scanning electron microscopy (SEM) investigations. It combines a SEM with a focused ion beam (FIB) column in one device. For energy dispersive X-ray spectroscopy (EDX) the device Apollo XP from EDAX (Ametek GmbH, Wiesbaden, Germany) was used. The measurement and analysis was done using the software Genesis Spectrum from EDAX. For EBSD the DigiView detector from EDAX was used. Data acquisition and analysis is accomplished by the EDAX software TSL-OIM. 2D EBSD mappings on FIB processed cross-sections were performed on single particles of the Ti-45Al-10Nb alloy with diameters of roughly 20, 40 and 100 µm.

RESULTS AND DISCUSSION

Phase compositions

The phase compositions determined by HEXRD are shown in figure 2.

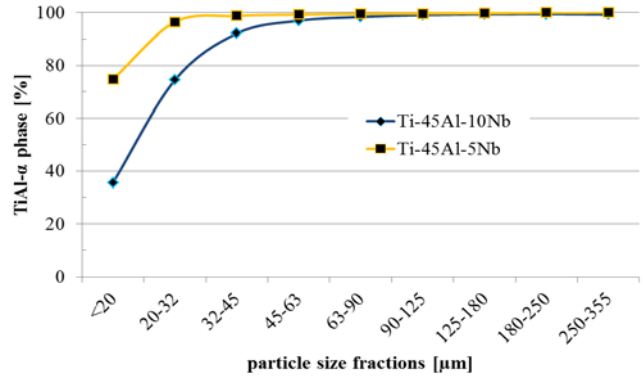

Figure 2: α-Ti(Al)-phase fraction of Ti-45Al-5Nb & Ti-45Al-10Nb powder fractions in volume percent.

The dominant phase constituent in almost every powder particle size fraction that was investigated is either disordered hexagonal close packed α-Ti(Al)-phase (A3 structure) or its ordered counterpart α_2-Ti_3Al-phase ($D0_{19}$ structure). Considerable amounts of body centered cubic β-Ti(Al- phase (A2 structure) were only found in size fractions smaller than 32 µm and smaller than 45 µm for Ti-45Al-5Nb and Ti-45Al-10Nb respectively. With increasing particle diameter the amount of α/α_2-phase increases (fig. 2 and 3a). This is caused by the decreased cooling rate of the bigger powder particles, providing more time to reach a lower temperature phase constitution.

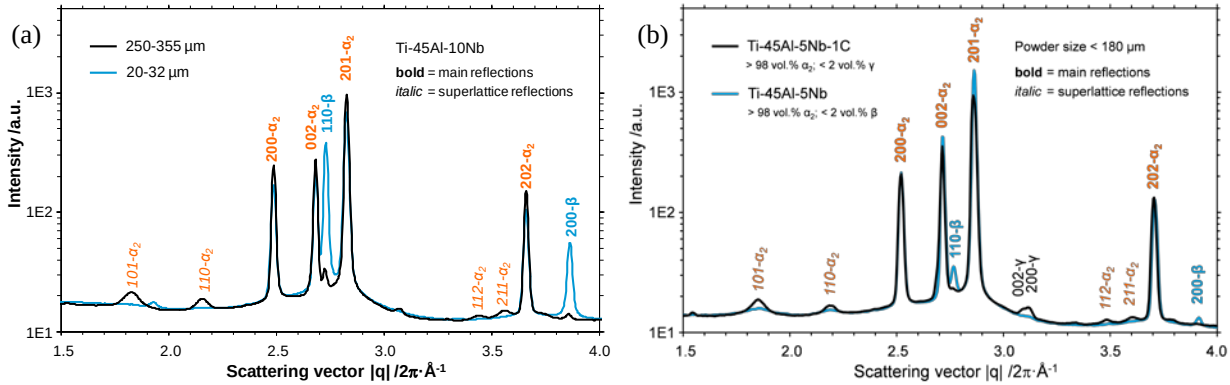

Figure 3: Diffraction patterns of: (a) Ti-45Al-10Nb with superlattice peaks of the α_2-phase (*101*-, *110*-, *112*- and *211*-α_2); (b) C stabilises the α_2-phase, shown by comparison of Ti-45Al-5Nb and Ti-45Al-5Nb-1C diffraction patterns.

Nb obviously stabilises the β-phase, resulting in a significantly higher amount of the β-phase in the alloy with 10 at% Nb, especially in the smallest particle size fractions (fig. 2). Additionally, the superlattice peaks indicating the presence of ordered α_2 instead of α-phase are slightly less pronounced in the alloy with 10 at% Nb. This effect is probably caused by the higher Nb amount, impeding the diffusion which is necessary for the ordering transformation $\alpha \rightarrow \alpha_2$.

Comparing different C contents, the alloy without C shows a small amount of the β-phase while in the alloy with 1 at% C the tetragonal γ-TiAl-phase ($L1_0$ structure) instead of the β-phase is visible (fig. 3b). In the particle size fractions < 180 µm the additional minor phases besides α/α_2 amount are less than 2 vol%. With increasing C content the amount of β is continuously decreasing while that of γ is growing. Additionally the α-phase starts to order indicated by the increasing intensity of the α_2 superlattice reflections with increasing C content (fig. 3b). This indicates that C stabilizes the α_2-phase against α-phase.

Nevertheless, the α_2 superlattice reflections (101-, 110-, 112- and 211-α_2) are always significantly less intensive than those expected for an ideal stoichiometrical order (fig. 3a,b). Comparing the integrated intensities of superlattice and main reflections, the degree of ordering can be estimated to be less than 50%. Additionally, the full width at half maximum (FWHM) of the superlattice reflections is significantly larger than that of the main reflections, indicating the relative small size of α_2-phase domains compared to the parent α-grains. In the smallest particle size fractions no α_2 superlattice reflections are visible (fig. 3a). This can be attributed to the extreme high cooling rate in the range of 10^5 K/s [1] which obviously provides not enough time for ordering.

Microstructure

All powder particle size fractions of the two alloys Ti-45Al-5Nb and Ti-45Al-10Nb were investigated by SEM imaging (fig. 4).

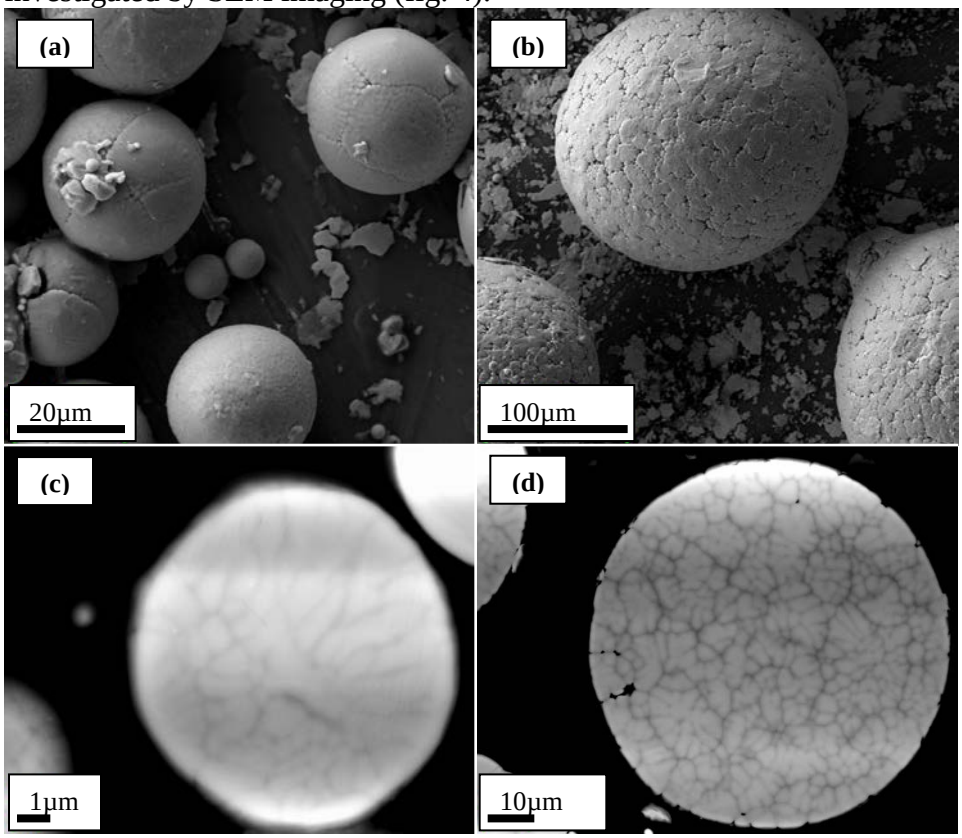

Figure 4: SEM images of (a) Ti-45Al-10Nb powder of the fractions 20-32 µm and (b) 180-250 µm; SE2-detector. (c) Cross-sections with dendrite structures of 12 µm and (d) 80 µm particles (diameter); BSE-detector.

A cauliflower-like structure was detected on the surface of the particles, which is almost equally sized and independent of the particle diameter (fig. 4a,b). By investigating cross-sections of particles using backscattered electron (BSE) contrast the continuation of these surface structures was detected as dendrites throughout the entire particles (fig. 4c,d). The structures in the powder particles stem from an inhomogeneous distribution of the alloying elements and imply that no planar solidification occurred. The composition differences of the darker interdendritic and the brighter dendrite core regions were measured by EDX [8]. The Nb distribution between both regions is more pronounced for bigger particles, while smaller particles seem to contain less pronounced Nb inhomogeneities. This means, the Nb depletion of the residual melt during β grain growth is the more pronounced the more time passes until complete solidification.

The α- and β-phases are crystallographically related by the Burgers orientation relationship. The α-grains growing from the same parent β-grain should thus be characterised by specific misorientation angles. However, no preferred misorientation angles were detected by EBSD measurements [8]. A very fast cooling from the single β-phase region can lead to a displacive martensitic transformation in Ti based and γ-TiAl based alloys [9]. However a martensitic transformation also would result in specific crystallographic orientation relationships and microstructural features which are not observed in the studied powders.

In order to analyse the α-Ti(Al)-phase grain structure, a three dimensional EBSD measurement of a powder particle with 100 µm diameter was performed (fig. 5).

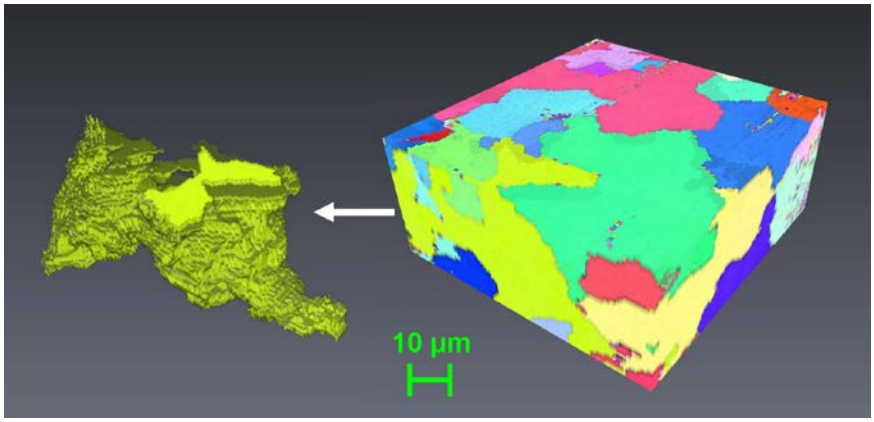

Figure 5: Cropped cube of 3D α-phase grain structure of a 100 µm sized Ti-45Al-10Nb particle, sliced by a 2 nA FIB current. The green grain was isolated out of the entire 3D body.

The grains are not arranged in accordance to the cauliflower-like structures detected by BSE inside the particles and no preferred crystal orientations with respect to the shape of the powder particle could be determined. A preferred growth direction was not observed and the grains even grew partially around each other. This microstructure can be attributed to a massive transformation.

CONCLUSIONS

We studied the microstructure of gas-atomised powders of several Nb-rich γ-TiAl based alloys by advanced microscopy and X-ray diffraction methods.

Initial β-grains were formed out of the melt during cooling. The dendritic cauliflower structure gives proof that diffusion took place during solidification and β-grain growth. The grain formation started from the cooler surface by several seeds, growing into the particle. The α-grains do not correlate to the dendritic structure of the primary β-grain and no obvious crystallographic orientation relationship to primary β-grains was found. The strong α-grain intergrowth indicates a massive β to α transformation.

The α/α_2-phase is the dominant phase in every powder fraction that was investigated. Considerable amounts of the β-phase were only observed in the smallest particle fractions. The total β-phase amount in Ti-45Al-10Nb fractions was generally higher, as expected for a higher Nb content. The high cooling rates significantly hamper the ordering transformation $\alpha \rightarrow \alpha_2$ and even can suppress the ordering as observed for the < 90 µm powder fractions.

ACKNOWLEDGMENTS

The authors thank Frank-Peter Schimansky and Dirk Matthiessen for producing the alloy powders and Michael Oehring for fruitful discussions.

REFERENCES

1 R. Gerling, H. Clemens, and F. P. Schimansky, Advanced Engineering Materials, 6 (2004), 23-38.

2 Bewlay, B.P., Weimer, M., Kelly, T., Suzuki, A., Subramanian, P.R., Materials Research Society Symposium Proceedings, 1516, (2013), 49-58. doi: 10.1557/opl.2013.44

3 Jabbar, H., Monchoux, J.-P., Houdellier, F., Dollé, M., Schimansky, F.-P., Pyczak, F., Thomas, M., Couret, A., Intermetallics, 18, (2010), 2312-2321. doi: 10.1016/j.intermet.2010.07.024

4 Gussone, J., Hagedorn, Y.-C., Gherekhloo, H., Kasperovich, G., Merzouk, T., Hausmann, J., Intermetallics, 66, (2015), 133-140. doi: 10.1016/j.intermet.2015.07.005

5 Baudana, G., Biamino, S., Klöden, B., Kirchner, A., Weißgärber, T., Kieback, B., Pavese, M., Ugues, D., Fino, P., Badini, C., Intermetallics, 73, (2016), 43-49. doi: 10.1016/j.intermet.2016.03.001

6 A. P. Hammersley, S. O. Svensson, M. Hanfland, A. N. Fitch, D. Hausermann, High Pressure Research 1996, 14, 235-248,

7 W. Kraus, G. Nolze, Journal of applied Crystallography 29 (1996), 301-303. doi: 10.1107/S0021889895014920

8 Laipple, D., Stark, A., Schimansky, F.-P., Schwebke, B., Pyczak, F., Schreyer, A., Key Engineering Materials, 704 (2016), 214-222. doi: 10.4028/www.scientific.net/KEM.704.214

9 Mayer, S., Petersmann, M., Fischer, F.D., Clemens, H., Waitz, T., Antretter, T., Acta Materialia 115 (2016), 242-249. doi: 10.1016/j.actamat.2016.06.006